

The effect of processing routes on the thermal and mechanical properties of poly(urethane-isocyanurate) nanocomposites

José María Kenny,¹ Luigi Torre,¹ Leonel Matias Chiacchiarelli²

¹Civil and Environmental Engineering Department, University of Perugia, UdR INSTM, 05100 Terni, Italy

²Instituto de Tecnología de Polímeros y Nanotecnología, CONICET, Engineering Faculty, University of Buenos Aires, AAR1124 Buenos Aires, Argentina

Correspondence to: L. M. Chiacchiarelli (E-mail: lmchiacchiarelli@yahoo.com.ar)

ABSTRACT: A systematic investigation of four processing routes was implemented so as to evaluate the thermal and mechanical properties of nanosilica (NS) reinforced poly(urethane-isocyanurate) nanocomposites (NC). The NS dispersion in the Polmix and the Iso-mix routes was performed in the polyol and the isocyanate precursor, respectively. The Isopol and the Solvmix routes consisted on the dispersion of the filler after the mixing of the precursors and with the aid of solvents, respectively. The NS dispersion, fractography (SEM, TEM), flexural and tensile mechanical properties, thermogravimetric analysis and FTIR analysis of NCs was performed as a function of processing route, isocyanate index, and NS concentration. Each route produced a NC with distinct properties, which were correlated to the NS agglomeration degree and how the NS affected the thermal transitions of the HS and the relative ratio of urethane and isocyanurate chemical groups. For example, the NC prepared with the Polmix route had substantial improvements of σ_t and ε_t of around +40 and +52%, respectively and an improved thermal resistance of the Hard Segments. © 2015 Wiley Periodicals, Inc. *J. Appl. Polym. Sci.* **2015**, *132*, 42750.

KEYWORDS: mechanical properties; nanocomposites; nanosilica; poly(urethane-isocyanurate); thermal properties

Received 18 May 2015; accepted 18 July 2015

DOI: 10.1002/app.42750

INTRODUCTION

The use of fillers with dimensions in the nanometer scale (nanofillers) has led to the development of advanced matrix resins (nanocomposites) (NC). Improved mechanical, thermal, and electrical properties can be achieved without significant modifications of the rheological or chemical properties of the matrix. However, one of the most relevant disadvantages of NC is that an additional dispersion stage has to be introduced in the preparation procedure so as to break down the initially agglomerated filler into shapes which can be considered to have nanometric dimensions. Several reviews and books^{1–7} have dealt with the critical aspects towards the successful development of nanometric dispersions. The most relevant variables which are responsible for the dispersion state are mixing methods and procedure, filler compatibilization, and cure temperature (specially for polyurethanes). As far as the mixing method is concerned, several techniques have been applied. Ultrasonication, high shear mixing, calandring, tip sonication, and conventional stirring have been widely studied.^{7–14} Filler compatibilization has an essential role in the final dispersion of the filler and on the formation of the stress-transfer effect between matrix and filler. On the other side, cure temperature has also a relevant

role in segmented polyurethanes, where a change in its value might cause segregation of the hard segments (HS), altering the dispersion of the nanofiller.¹⁵ Finally, several mixing procedures have been developed for the preparation of thermoset NC,^{6,7,16–37} from now on denominated routes. The main difference among those is based on which precursor the filler is dispersed. For the case of thermoset polyurethanes, which is the scope of this work, those can be grouped according to the following classification.

The first group, denominated from now on as Polmix, consists on the preparation of a NC where the filler has been dispersed in the polyol component.^{16,38–42} Taking into account that the main free radicals in the polyol are of the hydroxyl type, the dispersion of fillers in the polyol is usually performed without any chemical reaction taking place. The most relevant variables which control dispersion degree are polyol viscosity, the matching of the hydrophobic character of the polyol and filler, filler concentration and mixing energy.⁷ The stability of the resultant colloidal dispersion is mainly controlled by pH, ionic strength, and filler concentration. The second group, from now on denominated Isomix, is based on the preparation of NC where the filler has been previously dispersed in the isocyanate

precursor.^{43–45} This route is also known in industry as the preparation of a prepolymer, but, in contrast, it is not frequently used in scientific literature because of the highly reactive nature of the isocyanate group. Most of the surface groups present on the filler might react with the isocyanate component, producing carbon dioxide, amines, urea's, and other by-products.⁴⁶ The third group, from now on denominated Isopol, is based on the simultaneous mixing of the filler with both the isocyanate and polyol components (one-shot technique). This route has been implemented by several authors.^{16,47–49} The development of inhibitor systems with elevated inhibition times has opened up the possibility to disperse the filler after the isocyanate and polyol components have been mixed. The main advantage of this route is related to the mixing time. Taking into account that all the precursors are simultaneously injected, the processing times are minimized. In contrast, the nanofiller dispersion degree is deteriorated by this lower processing time lapse. Finally, the last group, from now on denominated as Solvmix, consists on the use of solvents to aid the dispersion of the filler and its subsequent dispersion in the polyol component with a simultaneous removal of the solvent. This route has been extensively studied by several authors.^{17,19,21,24,32,47,50–52} Its main advantage is associated to the resultant dispersion of the filler in the matrix. An improved dispersion degree has been achieved with this route. In contrast, the main disadvantage is related to the solvent evaporation during cure, which might induce the formation of voids within the surroundings of the nanofiller or within the microstructure as well as environmental issues. It is important to emphasize that the vast majority of publications have used the Solvmix route to develop PU NC. Other dispersion procedures have been developed, such as sol-gel and in-situ polymerization.⁷ Nevertheless, those can be considered as combinations of the previously stated routes.

As far as the matrix of the NC is concerned, polyurethane has been extensively studied as a matrix to obtain a wide variety of advanced materials.^{1,7,31,53} However, recent formulations which possess very fast cure cycles have been developed, particularly for the automotive industry.^{54–57} Taking into account that high production volumes are required in that industry, it is of paramount importance to reduce significantly the cure cycle. In contrast to epoxy, polyester, vinyl-ester, or other matrices, a PU matrix has an inherent faster reaction rate mainly due to the highly reactive nature of isocyanates, particularly for formulations which are based on the formation of an interpenetrated network of urethane and isocyanurate groups (PUI). Up to now, these formulations have only been applied to cellular structures, but, recently, catalysts which promote selectively the trimerization of isocyanate instead of the formation of carbon dioxide have opened up the way to a new family of high performance solid thermoset materials. It is important to notice that the effect of the different processing routes on the properties of PUI as well as other PU matrices has not been done before.

In this work, the previously stated processing routes will be used to evaluate its effect on the dispersion, mechanical, thermal, and interphase properties of NS based PUI NCs. In addition,

the effect of concentration and isocyanate index will also be evaluated.

MATERIALS AND METHODS

Materials

NS was purchased from Evonik under the tradename Aerosil R8200. It consisted of hydrophobic fumed silica (99.8%) with a specific surface area of $135 \text{ m}^2 \text{ g}^{-1}$. Before each material preparation, it was dried at 80°C in an oven overnight. The polyester polyol had an OH number of $127 \text{ mg KOH g}^{-1}$ an acidity of $2.84 \text{ mg KOH g}^{-1}$ and a viscosity of 210 mPa s (at 25°C). The diisocyanate was a 4,4'-diphenylmethane modified with uretonomine, obtained under the tradename Suprasec and Jeffol, respectively. Before each experiment, the NCO number was corroborated using the standard method ASTM D 2572. 2-Butanone (MEK, ACS reagent, >99.0%) was purchased from Sigma-Aldrich.

Methods

The dispersion of the filler in the liquid precursor was performed with a Dispermat LC30 high shear mixing equipment. A Cowles stirring blade of 35 mm. diameter was used for mixing at elevated revolutions (up to 15,000 rpm). While mixing the filler, the temperature was fixed to 30°C and the vacuum was set to 40 mbar by means of a CDS vacuum accessory (Dispermat). A schematic showing the dispersion steps associated to each processing route is depicted in Figure 1. The dispersion procedure of the filler in the polyol precursor (Polmix) consisted on three successive steps; an initial high shear mixing at 12,000 rpm at ambient pressure for 15 min followed by an additional step of 5,000 rpm for 10 min under vacuum (40 mbar) and finally 60 min at 1,000 rpm with identical vacuum. Then, the isocyanate precursor was added and mixed for 10 min under vacuum (40 mbar) at 1,000 rpm. The reactive mixture was then poured into a closed aluminum mold, which was used to cure the composite at isothermal conditions (1 h at 70°C), obtaining plates of 2 mm. thickness. Postcure was performed in an oven at 180°C for 30 min. The dispersion procedure of the filler in the isocyanate precursor (Isomix) consisted of two steps; an initial high shear mixing for 10 min at 10,000 rpm under vacuum (40 mbar) and, afterward, mixing for 30 min at 1,000 rpm under identical vacuum. Cure and postcure was identical to the previous route. The third processing route (Isopol), consisted on mixing the isocyanate and polyol precursors at 1,000 rpm for 5 min under vacuum (40 mbar). Afterwards, the filler was added and mixed for 10 min at 15,000 rpm under vacuum (40 mbar) following an additional mixing step at 5,000 rpm under vacuum (40 mbar) for another 10 min. After this, the reactive mixture was cured using the previously explained procedure. The fourth processing route (Solvmix) consisted on the dispersion of the filler in MEK by means of a Vibra-Cell ultrasonic processor (VC750) equipped with a 13-mm standard probe. To achieve this, 1 g of filler was sonicated in 40 mL of MEK for 30 min with a power of 225 W. Afterwards, 25 g of polyol precursor were added and the mixture was stirred with the high shear mixing equipment for 10 min at 5,000 rpm under vacuum (600 mbar). Afterwards, it was mixed for 60 min at 1,000 rpm under vacuum (100 mbar). Then, the isocyanate precursor was added, following the common procedure of the other routes. It should be noticed that FTIR analysis

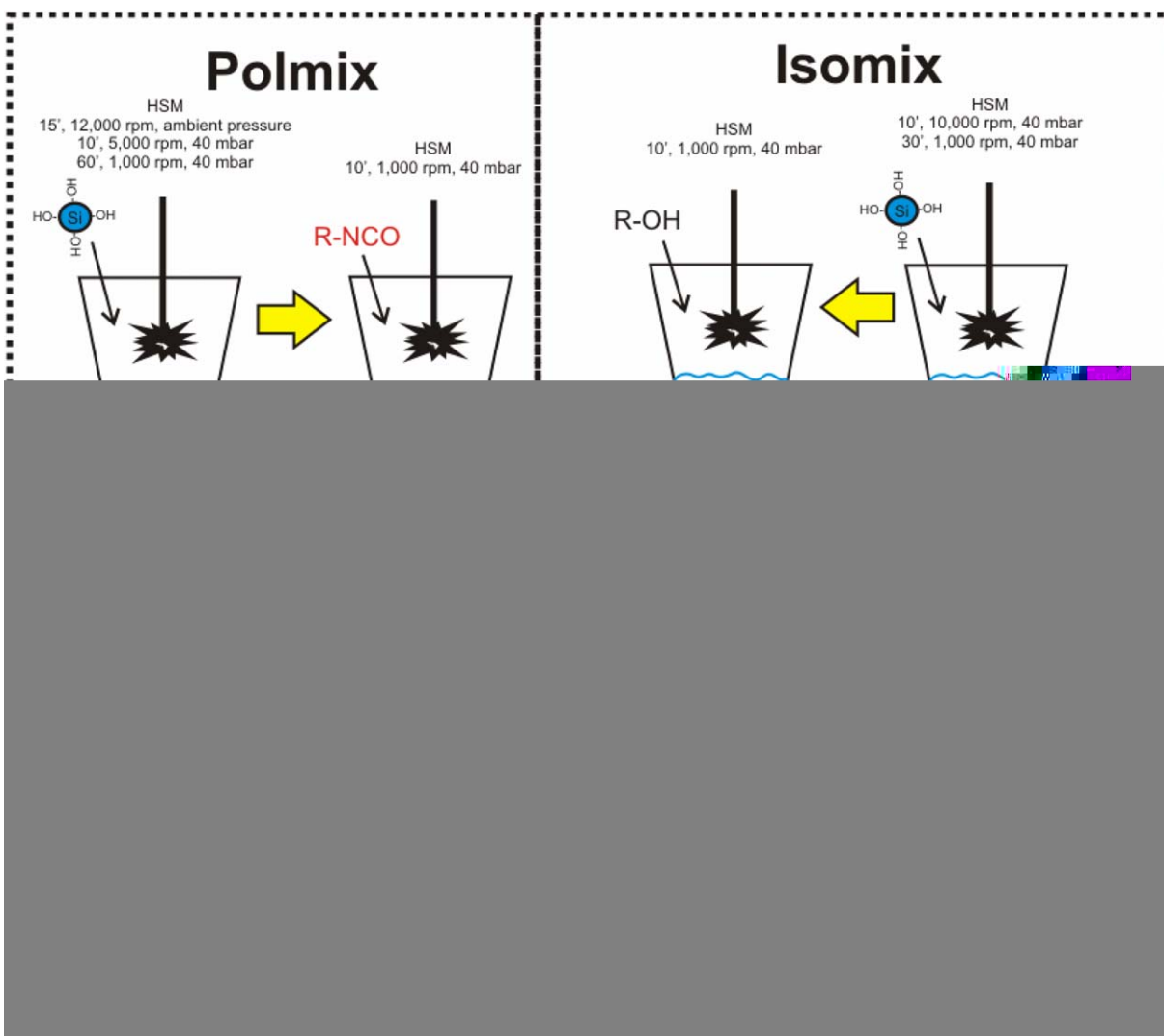


Figure 1. Processing routes used in this work to obtain $\text{Si}_7\text{-PUI}_x\text{ NC}$. [Color figure can be viewed in the online issue, which is available at wileyonlinelibrary.com.]

[Jasco IR-4000, attenuated total reflection (ATR) method] was used to corroborate that the vacuum and mixing stages effectively removed the MEK solvent.

For all processing routes, the weight ratio of isocyanate and polyol precursors ($w_{\text{iso}} : w_{\text{polyol}}$) were fixed to two values, 75 : 25 and 80 : 20 (pbw). These ratios are directly related to the index of the polyurethane formulation. Then, it can be inferred that a PUI prepared with a ratio of 80 : 20 will have a higher index with respect to the 75 : 25. With respect to nomenclature, PUI_1 and PUI_2 will refer to PUI prepared with 75 : 25 and 80 : 20 indexes, respectively.

To obtain samples for mechanical or thermal analysis, the PUI plates were machined with a computer numerical control device (Roland MODELA). By using this methodology, it was possible to obtain samples with virtually identical dimensions.

Tensile mechanical tests were performed with an Instron 3382 universal testing machine following the guidelines of the standard ASTM D3039. Flexure mechanical tests were performed

with a Lloyd Instruments LK30 following the guidelines of the standard ASTM D790. For each mechanical test, 10 samples were tested. It is important to point out that to corroborate that the results of each mechanical tests were reproducible; two plates were casted with each processing route. No significant differences (tensile or flexural tests) were found among plates prepared by an identical processing route.

Transmission electron micrographs (TEM) of the cured composite were done using a Philips EM-208 system. The micrographic information presented in this work was based on the observation of at least three micrographs at two magnifications, denoted as low magnification (LM, 11 kX) and high magnification (HM, 180 kX). Those magnifications were chosen because it was possible to distinguish the dimensions of agglomerates (LM) and the distances between the nanoparticles (HM). Scanning Electron Micrography (SEM) was performed with a Field Effect Supra 25-Zeiss (Germany). Thermogravimetric weight loss experiments were performed using a Seiko Exstar 6000. The samples were tested in a nitrogen atmosphere using a thermal

cycle, which started at 30°C and went up to 800°C at a heating rate of 5°C min⁻¹. The reproducibility was tested by measuring at least three samples. Dynamical mechanical thermal analysis (DMTA) was performed using an Ares N2 Rheometer in the torsion mode. The experiments were done using a temperature ramp from 30 to 300°C at a rate of 3°C min⁻¹. In addition, the frequency was set to 1 Hz and the strain to 0.1.

To evaluate the formation of urethane and isocyanurate groups in the samples of this work, the infrared absorption spectra of each of those was obtained. A Jasco IR-4000 Fourier Transformed Infrared Radiation (FTIR) equipment was used equipped with an ATR accessory. It should be noticed that the FTIR spectra of each sample was obtained, then, the specific area of the urethane and isocyanurate absorption bands was used to calculate the relative amounts of urethane and isocyanurate in each sample configuration. To avoid confusion, the FTIR absorption spectrum can be found in supporting information. All the samples prepared in this work had a null content of unreacted isocyanate, a fact that was determined through the analysis of the absorption band of isocyanate centered at 2275 cm⁻¹.

With respect to nomenclature, it is important to notice that the term PUI_{*i*} will refer to a poly(urethane-isocyanurate) (PUI) material with no filler in its formulation and with an index *i*. In contrast, Sil_{*p*}-PUI_{*i*} *x* wt % will refer to a NC prepared with the processing route *p* with *x* wt % of nanosilica (NS) filler and *i* index.

RESULTS AND DISCUSSION

Isocyanurate Crosslinking Degree

A typical PU structure is formed by two phases, the soft segment (SS) and the HS. The degree with which those phases are separated is evaluated by the determination of the free and bonded isocyanate groups.^{17,19,22,32,36} The isocyanate group has a carbonyl group, which is capable of interacting with other isocyanate groups through hydrogen type interactions. This arrangement is usually known as the HS, a partially ordered structure, which is the cause of substantial changes of the mechanical properties of the material (physical crosslinking). Then, taking into account that a free carbonyl group has an infrared vibration absorption at 1730 cm⁻¹ and that a hydrogen bonded carbonyl group has it at 1703 cm⁻¹,⁵⁸⁻⁶¹ the relative absorption intensities can be used to determine the degree of phase separation. Nonetheless, in highly crosslinked polyurethanes, such as the one used in this work, the hydrogen interaction among the isocyanate groups becomes of secondary importance, because the highly crosslinked molecular structure prevents the rearrangement of the HS. Taking into account that the isocyanurate groups are responsible of such elevated crosslinking degree, then, the presence of such groups can be evaluated by measuring the absorption spectra of the isocyanurate group. Taking into account that the structure of the polyurethane will be composed of isocyanurate and urethane groups, the relative ratio of absorption (*I*/*U*) can be interpreted as a measurement of the isocyanurate crosslinking degree. A higher *I*/*U* ratio will imply a structure with a higher content of isocya-

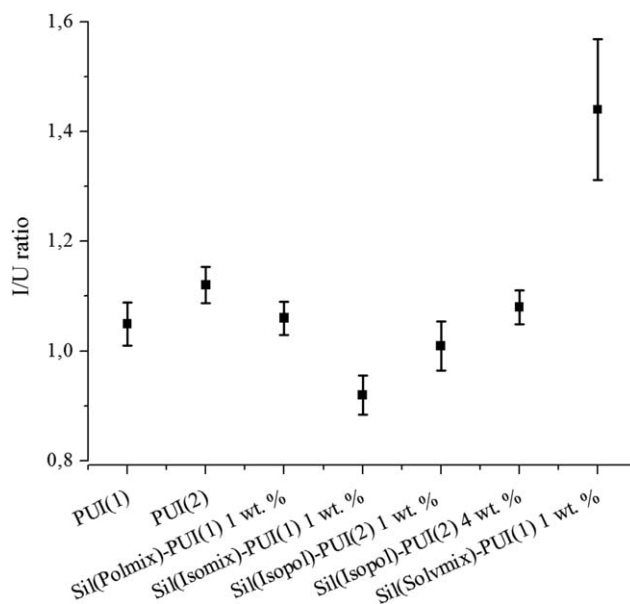


Figure 2. Isocyanurate-urethane (*I*/*U*) ratio obtained from FTIR analysis as a function of processing path, index, and NS concentration.

nurate groups with respect to the urethane group, which, in turn is associated to a more crosslinked network.

The relative ratio of infrared absorption of the isocyanurate and urethane groups *I*/*U* of the PUI₁, PUI₂, and the Sil_{*p*}-PUI_{*x*} prepared with different processing routes and filler concentrations is depicted in Figure 2.

Comparing the PUI₁ and PUI₂ it can be deduced that an increase of index produced a network with a higher content of isocyanurate groups. Then, it can be inferred that a higher crosslinking degree was attained. It should be noticed that, from a theoretical point of view, it was expected to obtain that result because an index increase would be translated in more available HS, which would in turn homopolymerize to form isocyanurate groups. As far as the effect of the processing route on the *I*/*U* ratio is concerned, relevant changes were found as a function of those. A substantial increase was measured for the Solvmix route, a neutral variation was measured for the Polmix route, and a decrease was measured for the Isomix and Isopol routes. It is important to emphasize the fact that the *I*/*U* ratio was related to the crosslinked degree of the NC, a higher *I*/*U* ratio implied a more crosslinked network. Finally, the effect of NS concentration on the *I*/*U* ratio is also depicted in Figure 2. As it can be deduced, an increase of NS concentration was correlated to an increase of the *I*/*U* ratio. The results found in this section are very relevant for subsequent discussions about the mechanical and thermal properties of the NCs. The reader will find in subsequent sections a contextualized discussion of these results.

It is important to notice that the scattering measured and depicted in Figure 2 had a relevant meaning. Due to the fact that the material tested with the FTIR analysis corresponded to several micrometric sized regions, it can be deduced that the scattering meant that the material had an *I*/*U* ratio which changed in the micrometer range. Then, it can be inferred that

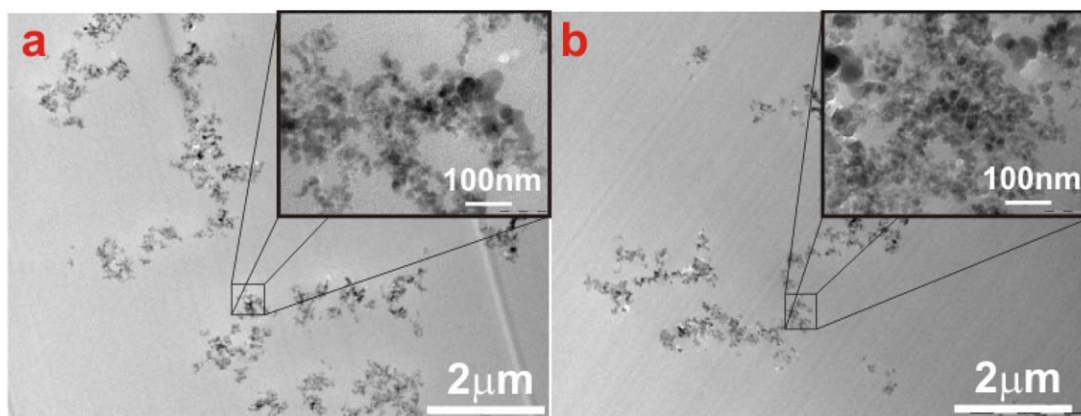


Figure 3. TEM micrographs of (a) $\text{Sil}_{\text{Polmix}}\text{-PUI}_1$ 1 wt % and (b) $\text{Sil}_{\text{Isopol}}\text{-PUI}_1$ 1 wt %. [Color figure can be viewed in the online issue, which is available at wileyonlinelibrary.com.]

the material had a microstructure composed of an interpenetrating network of isocyanurate and urethane groups where the specific ratio of each group fluctuated on a micrometer scale. Then, it can be concluded that the microstructure of the $\text{Sil}_{\text{SOLVMIX}}\text{-PUI}_1$ 1 wt % was, from a microscopic point of view, considerably heterogeneous.

NS Dispersion and Fractographic Behavior

The TEM micrographs showing the dispersion of $\text{Sil}_{\text{POLMIX}}\text{-PUI}_1$ 1 wt % and $\text{Sil}_{\text{Isopol}}\text{-PUI}_1$ 1 wt % are depicted in Figure 3(a,b), respectively. From a qualitative point of view, two main aspects can be deduced from Figure 3. The first one was related to how the NS formed agglomerated shapes, which could be discerned at low magnifications. The second one was related to the distances among each NS, which could only be discerned at elevated magnifications (insets of Figure 3). As already mentioned in previous publications,^{7,18,31,39} the mechanical and thermal properties are highly related on how the agglomerates and the interparticle distances vary as a function of processing routes and methods. However, one of the disadvantages of using TEM micrographs is that only geometrical aspects of the dispersion are considered. Due to the fact that the TEM specimen was microtomed, the correlation between fracture behavior and silica dispersion had been lost. Another relevant feature that was erased by the preparation procedure was the texture associated to the distribution of urethane and isocyanurate groups. It should be emphasized that the structure of the PUI used in this work was composed of an interpenetrating network of isocyanurate and urethane groups. Then, to circumvent both disadvantages, it was relevant to analyze SEM micrographs, where the features had not been erased by a previous preparation procedure.

The SEM micrographs of the fracture surface of the PUI_2 are depicted in Figure 4. The LM micrographs [Figure 4(a)] presented a smooth and uniform fracture surface, indicating a fragile behavior. In contrast, the HM micrographs [Figure 4(b)] presented a rough texture, indicating that, during fracture, the microstructure of the PUI_2 changed considerably the path of the growing crack. Specifically, the abrupt changes of brightness indicated also the presence of two phases. Taking into account

the interpenetrating nature of the PUI system, it was expected to have that feature.⁶²

The micrographs of the fracture surface of a $\text{Sil}_{\text{Polmix}}\text{-PUI}_2$ 1 wt % are depicted in Figure 4. The LM micrographs [Figure 4(c)] presented a rough texture, characterized by cracks propagating and leaving parabolic footprints. Then, it can be concluded that the NS reduced significantly the fragile nature of the PUI_2 , mostly by increasing the energy of crack propagation. In contrast, the HM [Figure 4(d)] micrographs revealed a smoother texture with respect to the PUI_2 . This fact indicated that the NS affected the nucleation and growth of the isocyanurate and isocyanurate networks, forming a finer nanostructure.

The micrographs of the fracture surface of a $\text{Sil}_{\text{Isopol}}\text{-PUI}_2$ 1 wt % are depicted in Figure 4. The LM micrographs [Figure 4(e)] revealed a rough texture characterized with parabolic footprints and NS particles. In contrast to the Polmix route, the Isomix route produced a fracture surface with a higher density of fracture planes, indicating that the crack was deviated more frequently, which indicated that the fragile nature of the PUI_2 was furtherly reduced. The HM micrographs [Figure 4(f)] revealed a fine nanostructure, with an interpenetrated network of polyurethane-isocyanurate similar to the PUI_2 .

The micrographs of the fracture surface of a $\text{Sil}_{\text{Solvmix}}\text{-PUI}_2$ 1 wt % are depicted in Figure 4. In contrast to the other processing routes, the LM micrographs [Figure 4(g)] presented a very distinct microstructure. Specifically, the NS were agglomerated into irregular shapes with dimensions in the order of 10 μm . The agglomerates were not compact enough so as to avoid the propagation of the crack within its cross section.³⁹ Moreover, the fact that the agglomerate did not possess a homogeneous distribution of NS contributed to a substantial modification of the deviation path of the growing crack. In addition, the HM micrographs [Figure 4(h)] showed that the nanostructure of the $\text{Sil}_{\text{Isopol}}\text{-PUI}_2$ had an intermediate roughness between the structures obtained from the Polmix or Isomix routes.

The micrographs of the fracture surface of a $\text{Sil}_{\text{Solvmix}}\text{-PUI}_2$ 1 wt % are depicted in Figure 4. From the LM micrographs [Figure 4(i)] it can be deduced that the elevated surface roughness contributed to a substantial decrease of the fragile nature of the



Figure 4. Fracture surface of (a) PUl₂ (11 kX), (b) PUl₂ (180 kX), Sil_{Polmix}-PUl₂ 1 wt % at (c) 11 kX, and (d) 180 kX, Sil_{Somix}-PUl₂ 1 wt % at (e) 11 kX, and (f) 180 kX, Sil_{Isopol}-PUl₂ 1 wt % at (g) 11 kX and (h) 180 kX, Sil_{Solvmix}-PUl₂ 1 wt % at (i) 11 kX and (j) 180 kX. [Color figure can be viewed in the online issue, which is available at wileyonlinelibrary.com.]

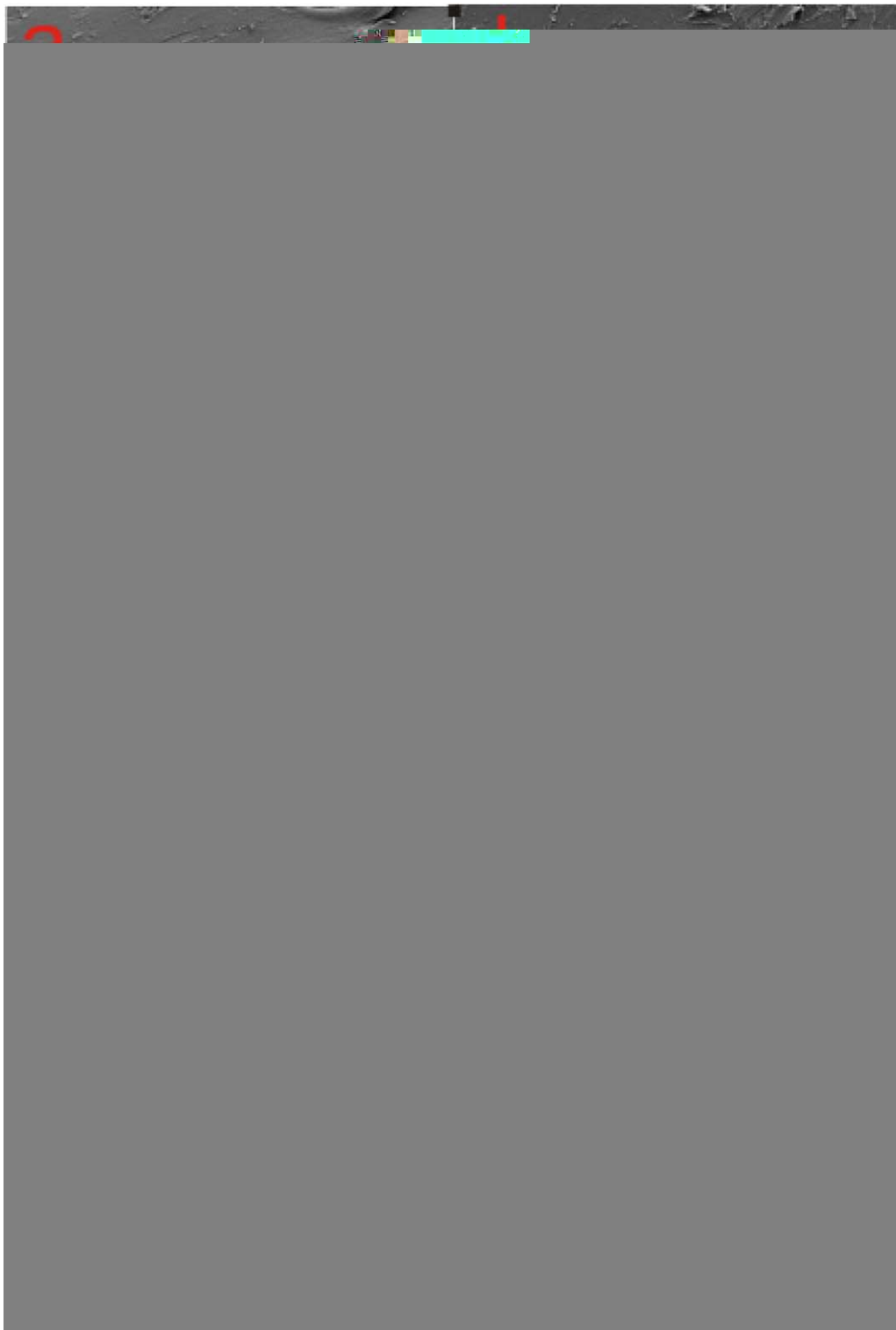


Figure 5. Fracture surface of (a) $\text{Si}_{\text{Polmix}}\text{-PUI}_2$ 1 wt %, (b) $\text{Si}_{\text{Polmix}}\text{-PUI}_2$ 2 wt %, (c) $\text{Si}_{\text{Isomix}}\text{-PUI}_2$ 1 wt %, (d) $\text{Si}_{\text{Isomix}}\text{-PUI}_2$ 4 wt %, (e) $\text{Si}_{\text{Isopol}}\text{-PUI}_2$ 1 wt %, (f) $\text{Si}_{\text{Isopol}}\text{-PUI}_2$ 4 wt %, (g) $\text{Si}_{\text{Solvmix}}\text{-PUI}_2$ 1 wt %, and (h) $\text{Si}_{\text{Solvmix}}\text{-PUI}_2$ 4 wt %. [Color figure can be viewed in the online issue, which is available at wileyonlinelibrary.com.]

PUI_2 . The main reason for this was related to the fact that the fracture surface was not mainly contained in a singular plane which but, instead, it was considerably extended to the direction perpendicular to the plane of the SEM micrograph. Then, it can

be deduced that the crack was originated at several points of the matrix and had a criss-cross propagation around several directions. However, the HM micrographs [Figure 4(j)] revealed that the NS were mostly agglomerated in irregular shapes with

Table I. Formulations Used for Tensile Tests

Processing route	Filler concentration (wt %)	Tensile modulus (GPa)	Tensile strength (Mpa)	Strain to failure (%)
PUI ₂	0	2.42+/-0.09	59.6+/-11.4	4.54+/-1.57
PUI ₁	0	2.04+/-0.14	82.6+/-10.1	6.88+/-1.32
Sil _{POLMIX} -PUI ₂	1	2.45+/-0.09	69.9+/-18.4	5.4+/-2.17
Sil _{POLMIX} -PUI ₂	2	2.09+/-0.06	83.5+/-5.71	6.90+/-1.07
Sil _{SOMIX} -PUI ₁	1	1.97+/-0.05	72.8+/-9.2	6.03+/-1.89
Sil _{SOMIX} -PUI ₂	1	1.83+/-0.08	70.7+/-2.3	6.39+/-1.01
Sil _{SOMIX} -PUI ₂	2	1.92+/-0.04	65.7+/-1.9	5.2+/-1.50
Sil _{SOMIX} -PUI ₂	4	2.03+/-0.08	62.3+/-11.8	4.02+/-1.63
Sil _{SOPOL} -PUI ₂	1	1.81+/-0.05	65.0+/-14.0	5.77+/-2.06
Sil _{SOPOL} -PUI ₂	2	1.94+/-0.15	75.6+/-3.3	6.4+/-1.1
Sil _{SOPOL} -PUI ₂	4	2.61+/-0.1	75.1+/-7	5.7+/-1
Sil _{SOLVMIX} -PUI ₁	1	1.99+/-0.03	65.3+/-17.9	4.87+/-2.19
Sil _{SOLVMIX} -PUI ₂	1	2.09+/-0.1	75.9+/-15	6.93+/-4.0
Sil _{SOLVMIX} -PUI ₂	2	1.97+/-0.35	70.9+/-27.8	8.57+/-4.8
Sil _{SOLVMIX} -PUI ₂	4	2.03+/-0.1	71.9+/-12.1	5.42+/-2.09

dimensions in the order of 100 nm. The most relevant feature of the nanostructure was the presence of voids surrounding the nanoparticles agglomerates, indicating the presence of a debonding and void growth fracture mechanism.

The effect of NS concentration on the fracture surface of the Sil_i-PUI₂ prepared with all the processing routes is depicted in Figure 5. For example, comparing the Sil_{POLMIX}-PUI₂ prepared with NS at 1 and 2 wt % it can be deduced that the fracture surface had coarser features, indicating that the NS had a more preponderant role in the modification of the fracture path of the matrix. In addition, no substantial changes were observed with respect to the dispersion of the NS, with no substantial agglomeration of those as a function of increasing NS concen-

tration. Similar conclusions can be drawn from the analysis of the effect of concentration on the NCs prepared with the other processing routes. Then, it can be concluded that a change in NS concentration did not change the mechanistic aspects of failure propagation but, rather, its intensity.

Tensile and Flexural Mechanical Properties

The tensile and flexural properties have been tested as a function of NS concentration, processing route, and isocyanate index. A summary of the tested formulations is depicted in Tables I and II. Taking into account that the effect of several variables has been studied, the results will be exposed in a parametric way, showing the effect of each variable separately.

Table II. Formulations Tested for Flexural Tests

Processing route	Filler concentration (wt %)	Flexural modulus (GPa)	Flexural strength (Mpa)	Max. Strain at max. (%)
PUI ₁	0	2.39+/-0.03	123+/-5.0	8.44+/-0.74
PUI ₂	0	2.43+/-0.09	135+/-7.6	8.77+/-0.89
Sil _{POLMIX} -PUI ₂	1	2.68+/-0.11	135+/-11	7.74+/-1.6
Sil _{POLMIX} -PUI ₂	2	2.45+/-0.05	104.5+/-26	6.06+/-2.4
Sil _{SOMIX} -PUI ₂	1	2.21+/-0.02	109+/-14	8.06+/-2.05
Sil _{SOMIX} -PUI ₁	1	2.30+/-0.04	118+/-5.0	8.09+/-1.08
Sil _{SOMIX} -PUI ₂	2	2.45+/-0.04	123+/-6.5	7.95+/-1.38
Sil _{SOMIX} -PUI ₂	4	2.55+/-0.02	132+/-9.8	7.71+/-1.25
Sil _{SOPOL} -PUI ₂	1	2.30+/-0.04	115+/-1.3	8.76+/-0.54
Sil _{SOPOL} -PUI ₂	2	2.35+/-0.02	127+/-1.2	9.42+/-0.35
Sil _{SOPOL} -PUI ₂	4	2.79+/-0.06	139+/-4.19	8.36+/-0.74
Sil _{SOLVMIX} -PUI ₁	1	2.35+/-0.02	117+/-5.8	6.92+/-0.98
Sil _{SOLVMIX} -PUI ₂	1	2.50+/-0.19	134+/-0.79	8.84+/-0.32
Sil _{SOLVMIX} -PUI ₂	2	2.51+/-0.04	133+/-6.95	8.37+/-1.01
Sil _{SOLVMIX} -PUI ₂	4	2.40+/-0.02	126+/-2.5	8.61+/-0.58

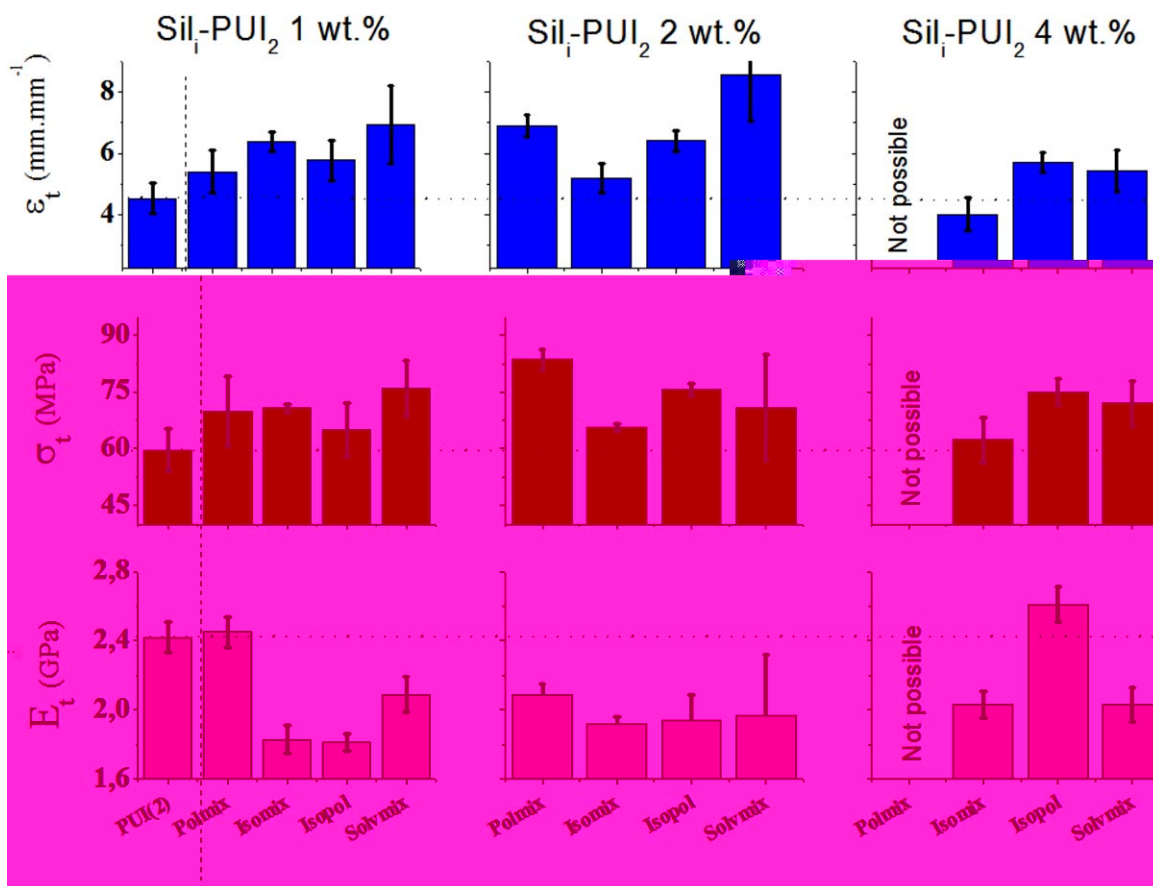


Figure 6. Effect of NS concentration and processing route on the strain to failure (ϵ_t), tensile strength (σ_t), and elastic modulus (E_t) of the PUI₂ NC under tensile stress. [Color figure can be viewed in the online issue, which is available at wileyonlinelibrary.com.]

The effect of processing route and filler concentration on the tensile properties of the NCs is depicted in Figure 6. The first, second, and third row in Figure 6 shows the strain to failure (ϵ_t), tensile strength (σ_t), and tensile modulus (E_t), respectively. Within each row, the first, second, and third graph (starting from the left) shows the results associated to filler concentrations of 1, 2, and 4 wt %, respectively. Within a graph, each column represents a NC prepared with one specific processing route. The only exception is the first column of the left, where the properties of the PUI₂ were depicted. Taking into account that these results were the baselines of the study, for comparison purposes, horizontal line associated to the properties of the PUI₂ has been drawn within each row.

As far the effect of concentration and processing route on the tensile modulus (E_t) is concerned (third row of Figure 6), the general conclusion that can be stated is that the E_t was slightly deteriorated as a function of those variables. Taking into account the effect of concentration by itself, it can be inferred that a concentration increase caused a general null or detriment effect on E_t . The only exception was the Isopol route, where a monotonous increase of E_t was measured as a function of concentration. Introducing the processing route variable into the analysis, comparing each column of the third row of Figure 6 it can be deduced that the processing route had a strong effect on the E_t . A strong variation of E_t was measured as a function of processing route. Specifically, a strong scattering was found for the NCs prepared with the

Solvmix route. Taking into account the results obtained in previous sections, it was logical to obtain that response.

As far as the effect of concentration and processing route on the tensile strength (σ_t) is concerned (second row of Figure 6), the general conclusion that can be stated is that a general improvement of σ_t was measured as a function of those variables. However, the specific increase depended substantially on both concentration and processing route. If only concentration is considered in the analysis, the improvement of σ_t was found to behave in a parabolic way, where the maximum was centered at a concentration of 1 wt %. This behavior was consistent for all processing routes. In contrast, considering only the effect of the processing route, it was found that the Polmix route achieved the highest σ_t . In contrast to the other processing routes, the Solvmix produced a relevant scattering.

As far as the effect of concentration and processing path on strain to failure (ϵ_t) is concerned (first row of Figure 6), an overall increase as a function of processing route and concentration was measured. Considering the effect of concentration by itself, the change of ϵ_t followed a parabolic trend (similar to the σ_t). The maximum ϵ_t was associated to the Solvmix processing route with a filler concentration of 2 wt %. Considering the effect of processing route by itself, substantial changes of ϵ_t were measured as a function of that variable. Specifically, the Solvmix route produced a relevant scattering.

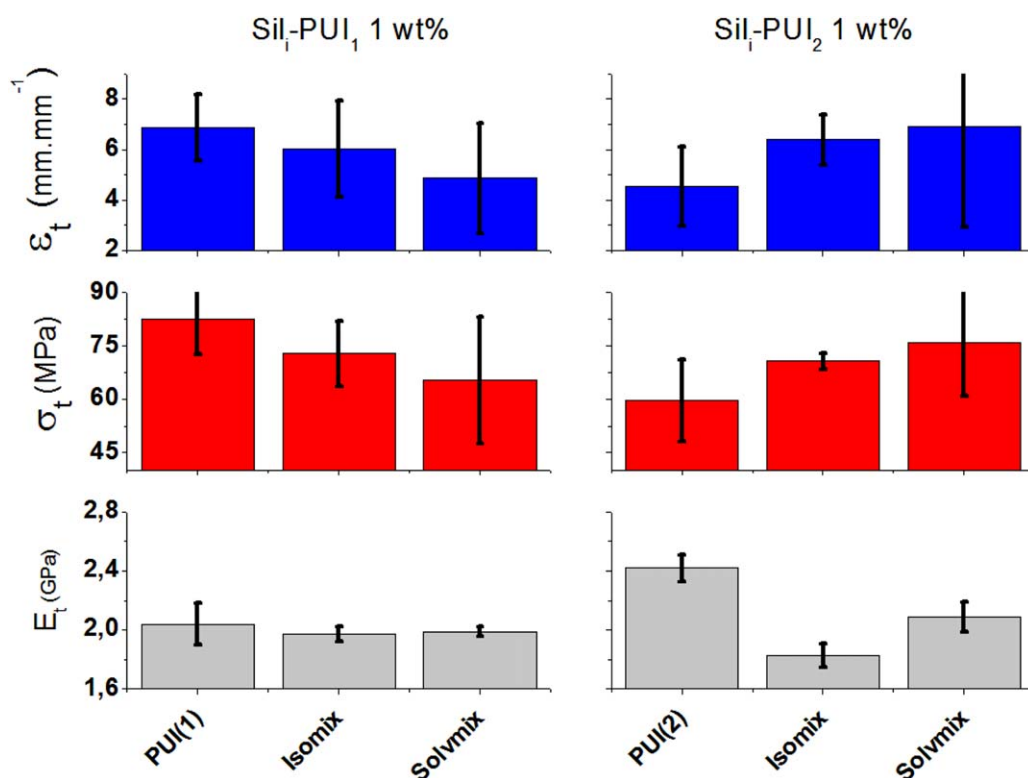


Figure 7. Tensile mechanical properties of the NC as a function of index and processing route with a NS concentration fixed to 1 wt %. [Color figure can be viewed in the online issue, which is available at wileyonlinelibrary.com.]

The effect of the isocyanate index and the processing route on the tensile properties of the NCs is depicted in Figure 7. The ϵ_t , σ_t , and E_t are depicted in the first, second, and third rows of Figure 7, respectively. In addition, the columns of the left and right show the mechanical properties of NCs with indexes 1 and 2, respectively. Within each graph, the first column refers to the PUI_x while the adjacent refer to Sil_i-PUI_x processed with different routes (to avoid confusion, only two processing routes were depicted).

As far as the ϵ_t is concerned, the effect of index and processing route is depicted in the first row of Figure 7. For the case of the PUI_x, a decrease of ϵ_t was measured as a function of increasing index. In contrast, for the Sil_i-PUI_x prepared with the ISOMIX and SOLVMIX routes, the exact opposite trend was measured. The ϵ_t increased as a function of increasing index. As far as the σ_t is concerned, the effect of the index and processing route is depicted on the second row of Figure 7. It should be noticed that the effect of those variables on σ_t was identical to what was measured for ϵ_t .

As far as the E_t is concerned, the effect of the index and processing route is depicted in the third row of Figure 7. Considering the effect of index by itself, for the case of the PUI_x, the E_t increased significantly as a function of increasing index (+20%). In contrast, for the Sil_i-PUI_x prepared with the Isomix and Solvmix routes, the index had an insignificant effect on the E_t .

The previous results have highlighted the effect of processing route, filler concentration, and index on the tensile properties

of the NCs. The tensile properties were specifically evaluated so as to have a general behavior of the material under a uniaxial load. However, it is important to evaluate the performance of the NCs under different stress conditions. For this reason, flexure tests were also performed and the results are described below.

The flexure and tensile properties of the PUI₂ and the Sil_i-PUI₂ processed with different routes are depicted on the left and the right column of Figure 8, respectively. The ϵ , σ , and E are showed in the first, second, and third row of Figure 8. Within each graph, the mechanical properties of the PUI₂ are depicted in the first column (starting from the left). The mechanical properties of the Sil_i-PUI₂ as a function of the processing route can be found in adjacent columns. As far as the PUI₂ is concerned, the effect of stress state on the ϵ , σ , and E are depicted on the first column of each graph. For the case of the E (third row of Figure 8), it is worthy to point out that the stress state had no effect on its value. In contrast, for the case of ϵ and σ , the introduction of the compression component into the analysis helped to improve the performance of the material. It is relevant to point out that the numerical values of any flexural or tensile property are not directly comparable. However, taking into account that both the ϵ and σ improved from the tensile state to the flexural state, it can be deduced that the flexural performance of the PUI₂ was improved with respect to the tensile one. For the case of the Sil_i-PUI₂ processed with the Polmix, Isomix, Isopol, and Solvmix routes, a similar behavior was found comparing the tensile and flexural properties. However, even though the E of PUI₂ was mostly unaltered by the stress

Figure 8. Tensile and Flexural mechanical properties as a function of processing route for the NC prepared at a fixed NS concentration of 1 wt %. [Color figure can be viewed in the online issue, which is available at wileyonlinelibrary.com.]

state, for the case of the $\text{SiI}_7\text{-PUI}_2$, significant changes were found as a function of that variable. Specifically, the E_t was found to decrease substantially with respect to the E_f .

Thermogravimetric Weight Loss

The weight residue (WR) as a function of temperature for the PUI_x prepared with indexes 1 and 2 is depicted in Figure 9. Four degradation stages were identified. The most relevant ones were centered at a temperature of $\sim 350^\circ\text{C}$ (S1) and 400°C (S2), which can be associated to the thermal degradation of the HS and SS, respectively. Similar results have already been found for other PU systems.^{15,62–65} Two additional stages, centered at 150 and 500°C were also identified. The first one was associated to retained gases after cure while the second one was related to the thermal degradation of additives present in the PUI formulation. Comparing the WR of the two PUI_x systems prepared with different indexes, it can be inferred that an increasing index caused a higher thermal stability. In fact, the WR associated to the degradation stage centered at 350°C was shifted to higher temperatures ($+30^\circ\text{C}$). Similarly, the WR of the stage centered at 400°C was also shifted to higher temperatures. However, from the damping factor ($\text{Tan } \delta$) as a function of temperature plot it can be deduced that the index had a minimal effect on the urethane transition but a relevant effect on the one isocyanurate. As a matter of fact, the maximum of the $\text{Tan } \delta$ decreased as a function of decreasing index, indicating a better viscoelastic response or a tougher material. It is relevant to notice that this transition was also measured for temperatures above 200°C , where thermal degradation of the NC was possible. It should be noticed that these results were expected and can be explained based on the microstructure. As already

noticed before, the PUI system used in this work was designed to cure forming a highly crosslinked microstructure. The main cause of crosslinking is associated to the formation of isocyanurate groups. Taking into account that the isocyanurate groups are formed through the homopolymerization of isocyanate groups, then, a higher index would imply that a higher amount of free isocyanates were able to self-react and form isocyanurate groups. Then, a higher thermal stability and a decreased viscoelastic response would be expected because the isocyanurate groups have a greater thermal stability and rigidity with respect to the urethane groups formed by the chemical reaction of an

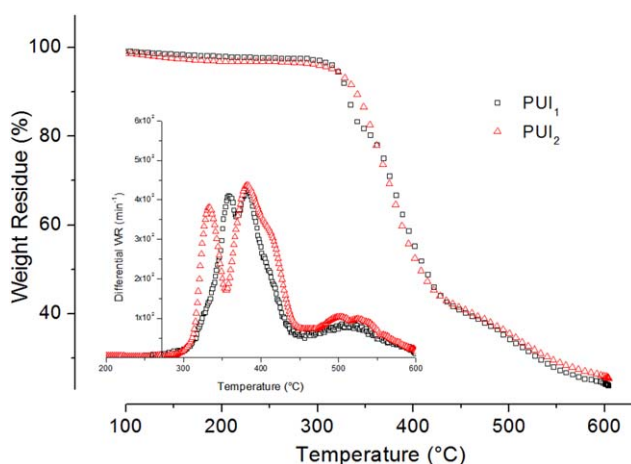


Figure 9. WR and differential WR as a function of temperature for PUI_x prepared with indexes 1 and 2. [Color figure can be viewed in the online issue, which is available at wileyonlinelibrary.com.]

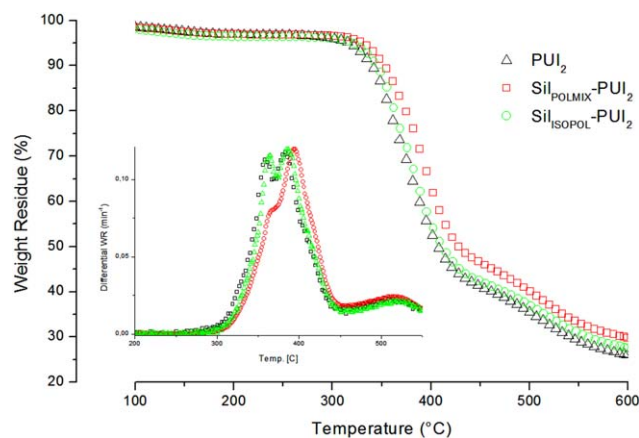


Figure 10. WR and differential WR as a function of temperature for PUI₂ and Sil_r-PUI₂ prepared with the Isopol and the Polmix processing route at a fixed NS concentration of 1 wt %. [Color figure can be viewed in the online issue, which is available at wileyonlinelibrary.com.]

isocyanate and polyol precursors.¹⁵ It is important to notice that, in the previous discussion, it was assumed that the WR was associated to the formation of urethane and isocyanurate chemical groups. This assumption was experimentally justified from the FTIR absorption spectra of the PUI presented in the previous section.

The WR as a function of temperature for a PUI₂ and Sil_r-PUI₂ prepared with the Isopol and Polmix routes is depicted in Figure 10. The NS concentration was fixed to 1 wt % and the index was 2. Based upon the previous discussion of the degradation stages, it can be deduced that only for the Sil_{Polmix}-PUI₂ the thermal stability improved. Specifically, the degradation stage S1 was not split and it was shifted to higher temperatures. Then, it can be deduced that the Polmix processing route produced a material with an isocyanurate network which had an improved thermal stability, even though its *I/U* ratio was not the highest one (Figure 2). Probably the NS hydrogen type

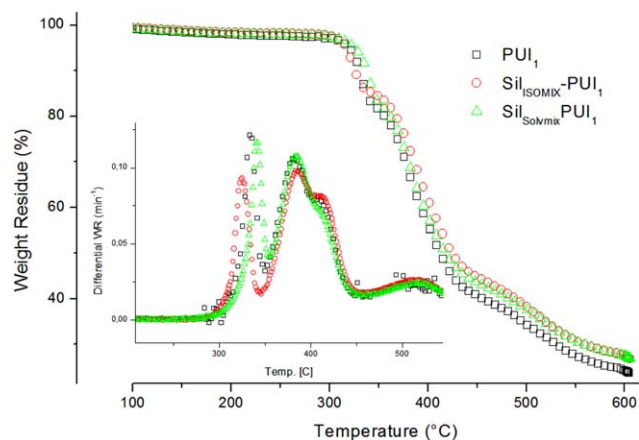


Figure 11. WR and differential WR as a function of temperature for PUI₁ and Sil_r-PUI₁ prepared with the Isomix and Solvmix processing routes and a NS concentration fixed to 1 wt %. [Color figure can be viewed in the online issue, which is available at wileyonlinelibrary.com.]

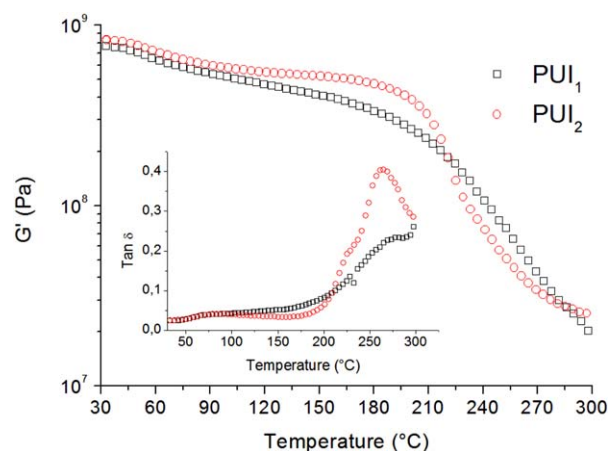


Figure 12. Elastic shear modulus (G') and damping factor ($\text{Tan } \delta$) as a function of temperature for the PUI₁ and PUI₂. [Color figure can be viewed in the online issue, which is available at wileyonlinelibrary.com.]

interactions improved the isocyanurate network thermal stability. In contrast, the Sil_{Isopol}-PUI₂ had a microstructure similar to the PUI₂.

The WR as a function of temperature for a PUI₁ and Sil_r-PUI₁ prepared with the Isomix and the Solvmix routes is depicted in Figure 11. The NS concentration was fixed to 1 wt % and the index to 1. Based upon the previous discussion about the thermal degradation stages, it can be deduced that the thermal stability of the PUI₂ and the Sil_r-PUI₂ prepared with the Isomix and Solvmix routes were similar.

In summary, the thermal stability of the PUI_x and the Sil_r-PUI_x was found not to change substantially as a function of processing routes. The only processing route that improved the thermal stability was the Polmix, due to the fact that additional hydrogen type interactions caused by the NS formed a more thermally stable isocyanurate network. As far as the index in concerned, an increase of the index was found to produce a microstructure with a higher content of isocyanurate groups, which ended up in an improved thermal stability.

Dynamical Mechanical Thermal Analysis

The elastic shear modulus (G') as well as the damping factor ($\text{Tan } \delta$), as a function of temperature for the PUI_x formulations prepared with indexes 1 and 2 are depicted in Figure 12. Regardless the index specific value, the variation of G' as a function of temperature indicated that two thermal transitions were present. The first one was centered at a temperature of $\sim 74^\circ\text{C}$ and the second one covered a wide region starting at 200°C and reaching temperatures of around 300°C . Taking into account the microstructure of the PUI used in this work, it was logical to obtain those transitions. The first one was associated to the glass to rubber transition (T_g) associated to the urethane network while the second one was associated to the isocyanurate network. It is important to emphasize that thermal degradation took place above 200°C (see Figure 9) which meant that the mechanical response was also affected by thermal degradation. The G' at 40°C for the PUI_x with indexes 1 and 2 were 752 and 815 MPa, respectively. Both decreased by one order of

magnitude (~ 20 MPa) when the temperature reached around 300°C . As far as the variation of G' as a function of temperature, a higher index implied a reduced rate of decrease of G' as a function of temperature. However, the variation of the damping factor as a function of temperature was also modified by a change of the formulation index. However, this change was only significant for the isocyanurate network transition region. In fact, the $\text{Tan } \delta$ increased for the PUI_2 with respect to the PUI_1 . The previous results can be understood based on the expected microstructure. The fact that the G' increased as a function of increasing index can be understood by the fact that a higher index formulation implied a microstructure with a higher isocyanurate content (see Figure 2). In addition, the fact that the $\text{Tan } \delta$ centered at a temperature of $\sim 250^\circ\text{C}$ was higher for the PUI_2 with respect to the PUI_1 indicated also that the microstructure had a detrimental elastic behavior, a fact to be expected taking into account that a higher content of isocyanurate groups would be present in the microstructure.

As far as the effect of processing route on the dynamic mechanical properties of the studied formulations, the G' and the $\text{Tan } \delta$ as a function of temperature is depicted in Figures 13 and 14. The NCs PUI_1 , $\text{Sil}_{\text{Polmix}}\text{-PUI}_1$ and the $\text{Sil}_{\text{Isopol}}\text{-PUI}_1$ are depicted in Figure 13. The formulations PUI_2 , $\text{Sil}_{\text{Polmix}}\text{-PUI}_2$, and the $\text{Sil}_{\text{Isopol}}\text{-PUI}_2$ are depicted in Figure 14. It is important to notice that the thermal transitions described above were also present in the previous graphs. From the results, it can be deduced that the processing route did not have a relevant effect on the thermal transition associated to the urethane network. In contrast, the thermal transition associated to the isocyanurate network changed, but to an extent that depended on the specific processing route. The most relevant result was associated to the Isopol route, were a relevant increase of

also improved, following a similar trend to what has been found for the Solvmix route.

The Isomix route proved to form NCs with a higher fracture resistance due to the deflection of the crack from its original propagation plane (Figure 4). This was translated in a NC with improved mechanical properties, but to an extent, which was not higher with respect to the other processing routes. For a NS concentration of 1 wt %, improvements of the σ_t and ε_t of +18.6 and +41% were found, respectively. Even though the improvements were not comparable to the other processing routes, it is important to emphasize that those improvements were measured for the lowest NS concentration. As far as the thermomechanical properties were concerned, a general detrimental effect was measured for the NCs prepared with this processing route. As a matter of fact, the temperature location of the $\tan \delta$ decreased with respect to the Neat-PUI as well as the G' absolute value.

The Polmix route proved to have the highest improvement in the σ_t of the NCs, as well as significant improvements of ε_t . Particularly, for a NS concentration of 2 wt %, an improvement of +40.1 and +52.0% was measured for σ_t and ε_t , respectively. These results can be associated to the fractured surface of the NC. As it was mentioned before (section "NS dispersion and fractographic behavior"), the Polmix route presented a rough texture, with cracks leaving behind a parabolic footprint. Then, the NS reduced significantly the fragile nature of the PUI by increasing the energy of crack propagation.

CONCLUSIONS

The effects of the processing routes have indicated that NCs with properties which can be tailored according to specific design requirements can be thus obtained. To that effect, the processing routes, the isocyanate index, and the NS concentration have played a fundamental role.

The dispersion of the NS in the PUI matrix changed considerably as a function of processing route. The incorporation of NS and the specific processing route affected both the agglomeration degree and the nucleation and growth of the isocyanurate and urethane networks. The Solvmix route was found to modify substantially the fracture surface of the NC, incorporating the debonding and growth fracture mechanism, which implied a relevant increase in the fracture resistance of the NC. However, the Isopol route contributed to the formation of NS agglomerates, which were not compact enough to avoid the deflection of growing cracks, hence, improving the fracture resistance of the NC by a matrix toughening mechanism. The Isomix route proved to form NC with a higher fracture resistance due to the deflection of the crack from its original propagation plane.

As far as the tensile mechanical properties are concerned, the processing routes had a general detriment effect on the E_t of the NC, regardless of the processing route. The only case where an improvement was measured was for the Isopol route, where a consistent improvement of E_t was measured as a function of increasing concentration. In contrast, the σ_t improved substantially as a function of processing routes, having a general maximum improvement at NS concentrations of 2 wt %. The

Polmix route proved to have the highest improvement in the σ_t of the NC. This was associated to the formation of a fractured surface with cracks, which left behind parabolic footprints. Finally, the ε_t changed considerably as a function of processing route, having maximum values at concentrations of around 2 wt %. In contrast to σ_b , the maximum value of ε_t was obtained for the Solvmix processing route. The comparison of the flexural and tensile mechanical properties have revealed that the effect of the studied variables had similar tendencies, except for the case of the E , where its tensile counterpart was found to be lower with respect to its flexural one.

The thermal resistance of the NC was found not to change substantially as a function of processing route. Only for the case of the Polmix route, an increase of the thermal stability of the HS was found, indicating a probable migration of the NS to the HS microstructure.

The thermal transitions (T_g) of the urethane and isocyanurate networks were modified by both the processing route and the index. As far as the urethane transition is concerned, no significant changes were observed as a function of index and processing route. However, for the case of the isocyanurate network, a decreasing index caused the formation of a material with an improved viscoelastic response (toughness). In addition, the Isopol route had a relevant role in changing the thermal transition of the isocyanurate network, improving substantially the damping capacity of the NC. This result can be correlated to the specific NS distribution and fracture surface as well as the mechanical properties, which accounted for a possible improvement of those properties. However, taking into account that incipient degradation of the material took place for temperatures above 200°C, it was difficult to discern if the changes of the thermal transitions were due to the processing route or to geometrical changes associated to the thermal degradation of the PUI matrix.

ACKNOWLEDGMENTS

Part of the work performed in this publication was funded by the European Union Seventh Framework Programme (FP7/2007–2013) under the topic NMP-2009-2.5-1, as part of the project HIVOCOMP (grant agreement no. 246389).

REFERENCES

1. Hussain, F.; Hojjati, M.; Okamoto, M.; Gorga, R. E. *J. Compos. Mater.* **2006**, *40*, 1511.
2. Shao-Yun, F.; Xi-Qiao, F.; Bernd, L.; Yiu-Wing, M. *Compos. B* **2008**, *39*, 933.
3. Jordan, J.; Jacob, K. I.; Tannenbaum, R.; Sharaf, M. A.; Jasiuk, I. *Mater. Sci. Eng. A* **2005**, *393*, 1.
4. Wang, Z.; Pinnavaia, T. J. *Chem. Mater.* **1998**, *10*, 3769.
5. LeBaron, P. C.; Wang, Z.; Pinnavaia, T. J. *Appl. Clay Sci.* **1999**, *15*, 11.
6. Ke, Y. C.; Stroeve, P. *Polymer-Layered Silicate and Silica Nanocomposites*; Elsevier Science: Amsterdam, The Netherlands, 1st ed.; **2005**.

7. Zou, H.; Wu, S. S.; Shen, J. *Chem. Rev.* **2008**, *108*, 3893.
8. Esposito Corcione, C.; Maffezzoli, A. *Thermochim. Acta* **2009**, *485*, 43.
9. Esposito Corcione, C.; Mensitieri, G.; Maffezzoli, A. *Polym. Eng. Sci.* **2009**, *49*, 1708.
10. Indennitate, L.; Cannoletta, D.; Lionetto, F.; Greco, A.; Maffezzoli, A. *Polym. Int.* **2010**, *59*, 486.
11. Franchini, E.; Galy, J.; Gérard, J.-F. *J. Colloid Interface Sci.* **2009**, *329*, 38.
12. Herrera-Alonso, J. M.; Marand, E.; Little, J. C.; Cox, S. S. *J. Membr. Sci.* **2009**, *337*, 208.
13. Ngo, T. D.; Ton-That, M. T.; Hoa, S. V.; Cole, K. C. *Compos. Sci. Technol.* **2009**, *69*, 1831.
14. Jin, J.; Chen, L.; Song, M.; Yao, K. *Macromol. Mater. Eng.* **2006**, *291*, 1414.
15. Randall, D.; Lee, S. *The polyurethanes book*; Wiley: United Kingdom, **2003**.
16. Zhou, S. X.; Wu, L. M.; Sun, J.; Shen, W. D. *Prog. Org. Coat.* **2002**, *45*, 33.
17. Torro-Palau, A. M.; Fernandez-Garcia, J. C.; Orgiles-Barcelo, A. C.; Martin-Martinez, J. M. *Int. J. Adhes. Adhes.* **2001**, *21*, 1.
18. Zhou, S. X.; Wu, L. M.; Sun, J.; Shen, W. D. *J. Appl. Polym. Sci.* **2003**, *88*, 189.
19. Petrovic, Z. S.; Cho, Y. J.; Javni, I.; Magonov, S.; Yerina, N.; Schaefer, D. W.; Ilavsky, J.; Waddon, A. *Polymer* **2004**, *45*, 4285.
20. Yang, C. H.; Liu, F. J.; Liu, Y. P.; Liao, W. T. *J. Colloid Interface Sci.* **2006**, *302*, 123.
21. Chen, X. C.; Wu, L. M.; Zhou, S. X.; You, B. *Polym. Int.* **2003**, *52*, 993.
22. Navarro-Banon, V.; Vega-Baudrit, J.; Vazquez, P.; Martin-Martinez, J. M. *Macromol. Symp.* **2005**, *221*, 1.
23. Kim, B. S.; Park, S. H.; Kim, B. K. *Colloid Polym. Sci.* **2006**, *284*, 1067.
24. Dubois, C.; Rajabian, M.; Rodrigue, D. *Polym. Eng. Sci.* **2006**, *46*, 360.
25. Chen, S.; Sui, J.; Chen, L. *Colloid Polym. Sci.* **2004**, *283*, 66.
26. Kang, S.; Hong, S. I.; Choe, C. R.; Park, M.; Rim, S.; Kim, J. *Polymer* **2001**, *42*, 879.
27. Hosgor, Z.; Kayaman-Apohan, N.; Karatas, S.; Menciloglu, Y.; Gungor, A. *Prog. Org. Coat.* **2010**, *69*, 366.
28. Tan, H. L.; Yang, D. Z.; Xiao, M.; Han, J.; Nie, J. *J. Appl. Polym. Sci.* **2009**, *111*, 1936.
29. Chen, G. D.; Zhou, S. X.; Liao, H. M.; Wu, L. M. *J. Compos. Mater.* **2005**, *39*, 215.
30. Seo, J. W.; Kim, B. K. *Polym. Bull.* **2005**, *54*, 123.
31. Chen, Y. C.; Zhou, S. X.; Yang, H. H.; Wu, L. M. *J. Appl. Polym. Sci.* **2005**, *95*, 1032.
32. Petrovic, Z. S.; Javni, I.; Waddon, A.; Banhegyi, G. *J. Appl. Polym. Sci.* **2000**, *76*, 133.
33. Chen, X. C.; You, B.; Zhou, S. X.; Wu, L. M. *Surf. Interface Anal.* **2003**, *35*, 369.
34. Xiang, X. J.; Qian, J. W.; Yang, W. Y.; Fang, M. H.; Qian, X. Q. *J. Appl. Polym. Sci.* **2006**, *100*, 4333.
35. Lee, S. I.; Hahn, Y. B.; Nahm, K. S.; Lee, Y. S. *Polym. Adv. Technol.* **2005**, *16*, 328.
36. Nunes, R. C. R.; Pereira, R. A.; Fonseca, J. L. C.; Pereira, M. R. *Polym. Test* **2001**, *20*, 707.
37. Kim, H.; Miura, Y.; Macosko, C. W. *Chem. Mater.* **2010**, *22*, 3441.
38. Chiacchiarelli, L. M.; Monsalve, L.; Vázquez, A.; Kenny, J. M.; Torre, L. *Polym. Eng. Sci.* **2014**, *54*, 1817.
39. Chiacchiarelli, L. M.; Puri, I.; Puglia, D.; Kenny, J. M.; Torre, L. *Colloid Polym. Sci.* **2013**, *1*.
40. Saha, M. C.; Kabir, M. E.; Jeelani, S. *Mater. Sci. Eng. A* **2008**, *479*, 213.
41. Zammarano, M.; Krämer, R. H.; Harris, R.; Ohlemiller, T. J.; Shields, J. R.; Rahatekar, S. S.; Lacerda, S.; Gilman, J. W. *Polym. Adv. Technol.* **2008**, *19*, 588.
42. Striebeck, N.; Li, X.; Kogut, I.; Moritz, H. U.; Eling, B.; Goerigk, G. J.; Hoell, A. *Macromol. Mater. Eng.* **2015**, *300*, 699.
43. Wu, Q.; Henriksson, M.; Liu, X.; Berglund, L. A. *Biomacromolecules* **2007**, *8*, 3687.
44. Rueda, L.; Fernández d'Arlas, B.; Zhou, Q.; Berglund, L. A.; Corcuera, M. A.; Mondragon, I.; Eceiza, A. *Compos. Sci. Technol.* **2011**, *71*, 1953.
45. Stankovich, S.; Piner, R. D.; Nguyen, S. T.; Ruoff, R. S. *Carbon* **2006**, *44*, 3342.
46. Szycher, M. *Szycher's Handbook of Polyurethanes*; CRC Press LLC: New York, **1999**.
47. Maciá-Agulló, T. G.; Fernández-García, J. C.; Torró—palau, A.; Orgilés Barceló, A. C.; Martín-Martínez, J. M. *J. Adhes.* **1995**, *50*, 265.
48. Benli, S.; Yilmazer, Ü.; Pekel, F.; Özkar, S. *J. Appl. Polym. Sci.* **1998**, *68*, 1057.
49. Yoon, S. H.; Park, J. H.; Kim, E. Y.; Kim, B. K. *Colloid Polym. Sci.* **2011**, *289*, 1809.
50. Nunes, R. C. R.; Pereira, R. A.; Fonseca, J. L. C.; Pereira, R. M. *Polym. Test* **2001**, *20*, 707.
51. Auad, M. L.; Contos, V. S.; Nutt, S.; Aranguren, M. I.; Marcovich, N. E. *Polym. Int.* **2008**, *57*, 651.
52. Wang, Y.; Tian, H.; Zhang, L. *Carbohydr. Polym.* **2010**, *80*, 665.
53. Radhakrishnan, B.; Ranjan, R.; Brittain, W. J. *Soft Matter* **2006**, *2*, 386.
54. Davies, G. *Materials for Automobile Bodies*; Butterworth-Heinemann: Oxford, **2003**.
55. Davies, G. *Materials for Automobile Bodies*; Butterworth-Heinemann: Oxford, **2012**.
56. Gebhard, A.; Hauptert, F.; Schlarb, A. K. *Tribology and Interface Engineering Series*; Klaus, F., Alois, K. S., Eds.; Elsevier: Amsterdam, The Netherlands, **2008**.

57. Sherman, A. M.; Krause, A.; Friedman, P.; Huston, D. Q. *Encyclopedia of Materials: Science and Technology*, 2nd ed.; Editors-in-Chief. K. H. J. B., Robert, W. C., Merton, C. F., Bernard, I., Edward, J. K., Subhash, M., Patrick, V., Eds.; Elsevier: Oxford, **2001**.
58. Yilgör, E.; Yilgör, I.; Yurtsever, E. *Polymer* **2002**, *43*, 6551.
59. Teo, L.-S.; Chen, C.-Y.; Kuo, J.-F. *Macromolecules* **1997**, *30*, 1793.
60. Brunette, C.; Hsu, S.; MacKnight, W. *Macromolecules* **1982**, *15*, 71.
61. Yu, X.; Nagarajan, M.; Li, C.; Gibson, P.; Cooper, S. *J. Polym. Sci. Part B: Polym. Phys.* **1986**, *24*, 2681.
62. Semsarzadeh, M. A.; Navarchian, A. H.; Morshedian, J. *Adv. Polym. Technol.* **2004**, *23*, 239.
63. Peng, S.; Fuchs, A. *Polym. Eng. Sci.* **2001**, *41*, 484.
64. Peng, S.; Jackson, P.; Sendijarevic, V.; Frisch, K. C.; Prentice, G. A.; Fuchs, A. *J Appl. Polym. Sci.* **2000**, *77*, 374.
65. Sun, X.; Toth, J.; James Lee, L. *Polym. Eng. Sci.* **1997**, *37*, 143.